An Analysis of SVD for Deep Rotation Estimation

Jake Levinson[1]   **Carlos Esteves**[2]   **Kefan Chen**[3]   **Noah Snavely**[3]
Angjoo Kanazawa[3]   **Afshin Rostamizadeh**[3]   **Ameesh Makadia**[3]
[1]University of Washington   [2]University of Pennsylvania   [3]Google Research

Abstract

Symmetric orthogonalization via SVD, and closely related procedures, are well-known techniques for projecting matrices onto $O(n)$ or $SO(n)$. These tools have long been used for applications in computer vision, for example optimal 3D alignment problems solved by orthogonal Procrustes, rotation averaging, or Essential matrix decomposition. Despite its utility in different settings, SVD orthogonalization as a procedure for producing rotation matrices is typically overlooked in deep learning models, where the preferences tend toward classic representations like unit quaternions, Euler angles, and axis-angle, or more recently-introduced methods. Despite the importance of 3D rotations in computer vision and robotics, a single universally effective representation is still missing. Here, we explore the viability of SVD orthogonalization for 3D rotations in neural networks. We present a theoretical analysis that shows SVD is the natural choice for projecting onto the rotation group. Our extensive quantitative analysis shows simply replacing existing representations with the SVD orthogonalization procedure obtains state of the art performance in many deep learning applications covering both supervised and unsupervised training.

1   Introduction

There are many ways to represent a 3D rotation matrix. But what is the ideal representation to predict 3D rotations in a deep learning framework? The goal of this paper is to explore this seemingly low-level but practically impactful question, as currently the answer appears to be ambiguous.

In this paper we present a systematic study on estimating rotations in neural networks. We identify that the classic technique of SVD orthogonalization, widely used in other contexts but rarely in the estimation of 3D rotations in deep networks, is ideally suited for this task with strong empirical and theoretical support.

3D rotations are important quantities appearing in countless applications across different fields of study, and are now especially ubiquitous in learning problems in 3D computer vision and robotics. The task of predicting 3D rotations is common to estimating object pose [47, 24, 29, 38, 43, 21, 39], relative camera pose [27, 32, 5], ego-motion and depth from video [48, 26], and human pose [49, 19].

A design choice common to all of these models is selecting a representation for 3D rotations. The most frequent choices are classic representations including unit quaternion, Euler angles, and axis-angle. Despite being such a well-studied problem, there is no universally effective representation or regression architecture due to performance variations across different applications.

A natural alternative to these classic representations is symmetric orthogonalization, a long-known technique which projects matrices onto the orthogonal group $O(3)$ [23, 35]. Simple variations can restrict the projections onto the special orthogonal (rotation) group $SO(3)$ [13, 18, 44]. This procedure, when executed by Singular Value Decomposition (SVD [9]), has found many applications in computer vision, for example at the core of the Procrustes problem [2, 35] for point set alignment, as

well as single rotation averaging [11]. A nearly identical procedure is used for factorizing Essential matrices [12].

Despite its adoption in these related contexts, orthogonalization via SVD has not taken hold as a procedure for generating 3D rotations in deep learning: it is rarely used when implementing a model (e.g. overlooked in [21, 5, 32, 26]), nor is it considered a benchmark when evaluating new representations [22, 50].

In light of this, this paper explores the viability of SVD orthogonalization for estimating rotations in deep neural networks. Note, we do not claim to be the first to introduce this tool to deep learning, rather our focus is on providing a comprehensive study of the technique specifically for estimating rotations. Our contributions include

- A theoretically motivated analysis of rotation estimation via SVD orthogonalization in the context of neural networks, and in comparison to the recently proposed Gram-Schmidt procedure [50]. One main result is that SVD improves over Gram-Schmidt by a factor of two for reconstruction, thus supporting SVD as the preferred orthogonalization procedure.

- An extensive quantitative evaluation of SVD orthogonalization spanning four diverse application environments: point cloud alignment, object pose from images, inverse kinematics, and depth prediction from images, across supervised and unsupervised settings, and benchmarked against classic and recently introduced rotation representations.

Our results show that rotation estimation via SVD orthogonalization achieves state of the art performance in almost all application settings, and is the best performing method among those that can be applied in both supervised and unsupervised settings. This is an important result given the prevalence of deep learning frameworks that utilize rotations, as well as for benchmarking future research into new representations.

2   Related Work

Optimization on $SO(3)$, and more generally on Riemannian manifolds, is a well-studied problem. Peculiarities arise since $SO(3)$ is not topologically homeomorphic to any subset of 4D Euclidean space, so any parameterization in four or fewer dimensions will be discontinuous (this applies to all classic representations—Euler angles, axis-angle, and unit quaternions). Discontinuities and singularities are a particular nuisance for classic gradient-based optimization on the manifold [37, 41].

Early deep learning models treated Euler angle estimation as a classification task [43, 38], by discretizing the angles into bins and using softmax to predict the angles. This idea was extended to hybrid approaches that combine classification and regression. In [20], discrete distributions over angles are mapped to continuous angles via expectation and [25] combines classification over quantized rotations with the regression of a continuous offset. In [22] it is shown that typical activations used in classification models (e.g. softmax) lead to more stable training compared to the unconstrained setting of regression. The authors introduce a "spherical exponential" mapping to bridge the gap and improve training stability for regression to n-spheres. All methods that discretize suffer from the problem of increased dimensionality and expressivity. All of the above methods require supervision on the classification objective, which makes them unsuitable for unsupervised settings.

Probabilistic representations have been introduced for modeling orientation with uncertainty [34, 8], with the von Mises and Bingham distributions respectively. While these are best suited for multimodal and ambiguous data, such approaches do not reach state of the art in tasks where a single precise rotation must be predicted.

The closest approach to SVD orthogonalization is the recent work of [50] which makes a strong connection between the discontinuities of a representation and their effect in neural networks. In search of continuous representations, they propose the idea of continuous overparameterizations of $SO(3)$, followed by continuous projections onto $SO(3)$. Their $6D$ representation is mapped onto $SO(3)$ via a partial Gram-Schmidt procedure. This is similar in spirit to SVD orthogonalization which will map a continuous 9D representation onto $SO(3)$ with SVD. We leave the deeper comparison of these two methods to the following sections, where we show that SVD provides a more natural projection onto $SO(3)$ in several respects (Section 3).

SVD derivatives have been presented in [7, 30], and there exist multiple works that build neural nets with structured layers depending on components of SVD or Eigendecomposition [16, 33, 15, 3, 28]. Close to our setting are [40] which applies the orthogonal Procrustes problem to 3D point set alignment within a neural network, and [17] which proposes singular value clipping to regularize networks' weight matrices.

SVD is amenable for learning via backpropagation. Its derivatives have been presented in [7, 30], and there exist multiple works that build neural nets with structured layers depending on SVD or Eigendecomposition [16, 33, 15, 3]. The closest to our setting is [40] which applies the orthogonal Procrustes problem to 3D point set alignment within a neural network, and [17] which proposes singular value clipping to regularize networks' weight matrices. We discuss the stability of SVD orthogonalization in neural networks in the following section.

3 Analysis

In this section we present our theoretically motivated analysis of SVD orthogonalization for rotation estimation. We start here defining the procedures and introducing well-known results regarding their least-squares optimality before presenting the analysis.

Given a square matrix M with SVD $U\Sigma V^T$, we consider the orthogonalization and *special* orthogonalization

$$\texttt{SVDO}(M) := UV^T, \tag{1}$$

$$\texttt{SVDO}^+(M) := U\Sigma'V^T, \text{ where } \Sigma' = \text{diag}(1, \ldots, 1, \det(UV^T)). \tag{2}$$

$\texttt{SVDO}$ is orientation-preserving, while $\texttt{SVDO}^+$ maps to $SO(n)$. Orthogonalization of a matrix via SVD is also known as *symmetric orthogonalization* [23]. It is well known that symmetric orthogonalization is optimal in the least-squares sense [2, 13, 35]:

$$\texttt{SVDO}(M) = \underset{R \in O(n)}{\arg\min} \|R - M\|_F^2, \qquad \texttt{SVDO}^+(M) = \underset{R \in SO(n)}{\arg\min} \|R - M\|_F^2. \tag{3}$$

This property has made symmetric orthogonalizations useful in a variety of applications [44, 35, 40].

To reiterate, the procedure for deep rotation estimation we will evaluate experimentally in Section 4 is $\texttt{SVDO}^+(M)$ in 3D, which takes a 9-dimensional network output (interpreted as a 3×3 matrix M), and projects it onto $SO(3)$ following Eq. 2.

3.1 $\texttt{SVDO}(M)$ and $\texttt{SVDO}^+(M)$ are maximum likelihood estimates

In this section we show that SVD orthogonalization maximizes the likelihood and minimizes the expected error in the presence of Gaussian noise. Let $M = R_\mu + \sigma N, M \in \mathbb{R}^{n \times n}$ represent an observation of $R_\mu \in SO(n)$, corrupted by noise N with entries $n_{ij} \sim \mathcal{N}(0, 1)$. Following from the pdf of the matrix normal distribution [10] the likelihood function is

$$L(R_\mu; M, \sigma) = ((2\pi)^{\frac{n^2}{2}} \sigma^{n^2})^{-1} \exp(-\tfrac{1}{2\sigma^2}((M - R_\mu)^T(M - R_\mu))). \tag{4}$$

$L(R_\mu; M, \sigma)$, subject to $R_\mu \in SO(n)$, is maximized when $(M - R_\mu)^T(M - R_\mu)$ is minimized:

$$\underset{R_\mu \in SO(n)}{\arg\max} L(R_\mu; M, \sigma) = \underset{R_\mu \in SO(n)}{\arg\min} (M - R_\mu)^T(M - R_\mu) = \underset{R_\mu \in SO(n)}{\arg\min} \|M - R_\mu\|_F^2 \tag{5}$$

The solution is given by $\texttt{SVDO}^+(M)$ (Eq. 3). Similarly, $\texttt{SVDO}(M)$ will minimize Eq. 4 when $R_\mu \in O(n)$.

3.2 Gradients

In this section we analyze the behaviour of the gradients of a network with an $\texttt{SVDO}^+$ layer, and show that they are generally well behaved. Specifically, we can consider $\frac{\partial L}{\partial M}$ for some a loss function $L(M, R) = \|\texttt{SVDO}^+(M) - R\|_F^2$. We will first analyze $\frac{\partial L}{\partial M}$ for $\texttt{SVDO}(M)$. Letting $\circ$ denote the

Hadamard product, from [16, 42] we have

$$\frac{\partial L}{\partial M} = U[(F \circ (U^T \frac{\partial L}{\partial U} - \frac{\partial L}{\partial U}^T U))\Sigma + \Sigma(F \circ (V^T \frac{\partial L}{\partial V} - \frac{\partial L}{\partial V}^T V))]V^T, \tag{6}$$

$$F_{i,j} = \begin{cases} \frac{1}{s_i^2 - s_j^2}, & \text{if } i \neq j \\ 0, & \text{if } i = j \end{cases}, \quad s_i = \Sigma_{ii} \tag{7}$$

Letting $X = U^T \frac{\partial L}{\partial U} - \frac{\partial L}{\partial U}^T U$, and $Y = V^T \frac{\partial L}{\partial V} - \frac{\partial L}{\partial V}^T V$, we see that X, Y are antisymmetric and $X = -Y$ (this is a result of the loss function depending on UV^T). We can reduce $\frac{\partial L}{\partial M} = UZV^T$ where the elements of Z are

$$Z_{ij} = \begin{cases} \frac{-X_{ij}}{s_i + s_j}, & \text{if } i \neq j \\ 0, & \text{if } i = j. \end{cases} \tag{8}$$

See Appendix C for the detailed derivation. For $\texttt{SVDO}(M)$ Eq. 8 tells us $\frac{\partial L}{\partial M}$ is undefined whenever two singular values are both zero and large when their sum is very near zero.

For $\texttt{SVDO}^+(M)$, if $\det(M) > 0$ then the analysis is the same as above. If $\det(M) < 0$, the extra factor $D = \mathrm{diag}(1, 1, \ldots, -1)$ effectively changes the smallest singular value s_n to $-s_n$. The derivation is otherwise unchanged. In particular the denominator in equation (8) is now $s_j - s_n$ or $s_n - s_i$ if either i or j is n. Thus, $\frac{\partial L}{\partial M}$ is undefined if the smallest singular value occurs with multiplicity greater than 1. It is large if the two smallest singular values are close to each other, or if they are close to 0.

3.3 Error analysis

In this section we approximate the expected error in $\texttt{SVDO}(M)$ and Gram-Schmidt orthogonalization (denoted as $\texttt{GS}(M)$) in the presence of Gaussian noise, and observe that the error is twice as large for $\texttt{GS}$ as for $\texttt{SVDO}$. If M is a matrix with QR decomposition $M = QR$, define:

$$\texttt{GS}(M) := Q, \qquad \texttt{GS}^+(M) := Q\Sigma'', \text{ where } \Sigma'' = \mathrm{diag}(1, \ldots, 1, \det(Q)). \tag{9}$$

We consider $M = R_0 + \sigma N$, a noisy observation of a rotation matrix $R_0 \in SO(n)$, where N has i.i.d. Gaussian entries $n_{ij} \sim \mathcal{N}(0, 1)$ and σ is small. Since $\det(M) > 0$ as $\sigma \to 0$, the analysis is identical for $\texttt{SVDO}^+$ and $\texttt{GS}^+$. The analysis is also independent of R_0 (Appendix A), so for simplicity we set $R_0 = I$. First we calculate the SVD and QR decompositions of M to first order for N an arbitrary (non-random) matrix.

Proposition 1 *The SVD and QR decompositions of $M = I + \sigma N$ are as follows:*

1. *(SVD) Let $N = S + A$ be the decomposition of N into symmetric and antisymmetric parts. Then, to first order, an SVD of M is given by*

$$M = U_0(I + \sigma U_1) \cdot (I + \sigma \Sigma_1) \cdot (I + \sigma V_1)^T U_0^T,$$

   where $U_0 \Sigma_1 U_0^T$ is an SVD of S, and U_1, V_1 are (non-uniquely determined) antisymmetric matrices satisfying $U_0^T A U_0 = U_1 + V_1^T$.

2. *(QR) Let $N = U + D + L$ be the strict upper-triangular, diagonal, and strict lower-triangular parts of N. To first order, M has QR decomposition*

$$M = (I + \sigma Q_1) \cdot (I + \sigma R_1),$$

   where $Q_1 = L - L^T$ and $R_1 = D + U + L^T$.

Consequently, $\texttt{SVDO}(M) = I + \sigma A + O(\sigma^2)$ and $\texttt{GS}(M) = I + \sigma(L - L^T) + O(\sigma^2)$.

Corollary 1 *If N is 3×3 with i.i.d. Gaussian entries $n_{ij} \sim \mathcal{N}(0, 1)$, then with error of order $O(\sigma^3)$,*

$$\mathbb{E}[\|\texttt{SVDO}(M) - I\|_F^2] = 3\sigma^2, \qquad \mathbb{E}[\|\texttt{GS}(M) - I\|_F^2] = 6\sigma^2 \tag{10}$$

$$\mathbb{E}[\|\texttt{SVDO}(M) - M\|_F^2] = 6\sigma^2, \qquad \mathbb{E}[\|\texttt{GS}(M) - M\|_F^2] = 9\sigma^2 \tag{11}$$

4

This corollary is by straightforward calculation since each entry of A and $L - L^T$ is Gaussian (see appendix A for the proof). Notably, Gram-Schmidt produces *twice* the error in expectation (and indeed deviates 1.5 times further from the observation M itself). The same holds for $\texttt{SVDO}^+$ and $\texttt{GS}^+$. This difference in performance can be traced to the fact that Gram-Schmidt is essentially "greedy" with respect to the starting matrix, whereas the SVD approach is coordinate-independent.

Although i.i.d. Gaussian noise is not necessarily reflective of a neural network's predictions, it does provide meaningful insight into the relationship between $\texttt{SVDO}^+$ and $\texttt{GS}^+$ and their relative performance observed in practice. See Appendix A for further remarks.

Proof of Proposition (sketch; see Appendix A for the full proof).

(1) Let M have SVD $M = USV^T$ for some orthogonal matrices U, V and diagonal matrix $S \geq 0$. To first order in σ, we can write

$$I + \sigma N = U_0(I + \sigma U_1)(S_0 + \sigma S_1)(I + \sigma V_1)^T V_0^T \tag{12}$$

with U_0, V_0 orthogonal, U_1, V_1 antisymmetric and $S_0, S_1 \geq 0$ diagonal. (This is using the fact that the antisymmetric matrices give the tangent space to the orthogonal matrices.) The claims come from breaking this equation into symmetric and antisymmetric parts; note if X is (anti-)symmetric and Q is orthogonal, then QXQ^T is again (anti-)symmetric. Simplify to get $\texttt{SVDO}(M) = I + \sigma A + O(\sigma^2)$.

For (2) the proof is similar: we expand the QR decomposition $M = QR$ to first order as

$$I + \sigma N = Q_0(I + \sigma Q_1)(I + \sigma R_1)R_0, \tag{13}$$

Q_0 orthogonal, Q_1 antisymmetric, and R_1, R_0 upper triangular; examine the upper and lower parts.

3.4   Continuity for special orthogonalization

The calculation above shows $\texttt{SVDO}(M)$ and $\texttt{SVDO}^+(M)$ are continuous and differentiable, at least at $M = I$. In fact $\texttt{SVDO}(M)$ is smooth, as is $\texttt{SVDO}^+$ except for a discontinuity[1] if (and only if) $\det(M) = 0$ or $\det(M) < 0$ and its smallest singular value has multiplicity greater than 1. In fact the optimization problem (3) is degenerate in this case. For example, the 2×2 matrix $M = \text{diag}(1, -1)$ is equidistant from every rotation matrix; perturbations of M may special-orthogonalize to any $R \in SO(2)$. $\texttt{GS}^+$ is continuous on a slightly larger domain – $\det(M) \neq 0$ – because it makes a uniform choice, negating the n-th column of M if necessary, at the cost of significantly greater error in expectation. This reflects the fact that SVD orthogonalization is coordinate-independent and $\texttt{GS}, \texttt{GS}^+$ are not:

$$\texttt{SVDO}(R_1 M R_2) = R_1 \texttt{SVDO}(M) R_2, \text{ for all } R_1, R_2 \in SO(n), M \in GL(n), \tag{14}$$

and similarly for $\texttt{SVDO}^+$. $\texttt{GS}$ and $\texttt{GS}^+$ are rotation-equivariant on only one side: $\texttt{GS}(R_1 M) = R_1 \texttt{GS}(M)$, but $\texttt{GS}(M R_2)$ is not a function of R_2 and $\texttt{GS}(M)$; likewise for $\texttt{GS}^+$. See Appendix B for a proof of smoothness and further discussion.

3.5   Summary

The results above illustrate a number of desirable properties of SVD orthogonalization. $\texttt{SVDO}^+$ is optimal as a projection in the least squares sense as well as in the presence of Gaussian noise (MLE). Viewed through the lens of matrix reconstruction, the approximation errors are half that of the Gram-Schmidt procedure. Finally we show the conditions that lead to large gradient norms (conditions that are rare for small matrices). In the following, we support this theoretical analysis with extensive quantitative evaluations.

4   Experiments

This section presents the experimental analysis for SVD orthogonalization and numerous baseline methods. To recap, the SVD orthogonalization procedure $\texttt{SVDO}^+(M)$ takes a 9D network output (interpreted as a 3×3 matrix), and projects it onto $SO(3)$ via Eq. 2. The procedure can easily be used in popular deep learning libraries (e.g. PyTorch [31] and TensorFlow [1] both provide differentiable SVD ops), and it does not affect efficiency (3×3 SVD adds negligible computational overhead in both forward and backward passes).

---

[1]If f is "discontinuous on a set S" of measure 0, it is equivalently "continuous on $\mathbb{R}^n \setminus S$."

Table 1: **3D point cloud alignment.** Left: a comparison of methods by *mean*, *median*, and *standard deviation* of (geodesic) errors after 2.6M training steps. Middle: mean test error at different points along the training progression. Right: test error percentiles after training completes. The legend on the right applies to both plots.

	Mean (°)	Med	Std
3D-RCNN	5.51	1.91	17.05
M_G	9.12	7.65	10.46
Euler	11.04	6.23	15.56
Axis-Angle	6.65	4.06	11.47
Quaternion	5.48	3.19	11.03
S^2-Reg	4.80	3.00	9.27
5D	3.77	2.19	8.70
6D	2.24	1.22	7.83
SVD-Inf	2.64	1.60	8.16
SVD-Train	**1.63**	**0.89**	**6.70**

Methods. Now we provide a short description of the methods under comparison (see Appendix D.1 for further details). **SVD-Train** is $\mathrm{SVDO}^+(M)$ (Eq. 2). **SVD-Inference** is $\mathrm{SVDO}^+(M)$, except the training loss is applied directly to M. Since SVDO^+ is applied only at inference, it is a continuous representation for training. **6D** and **5D** are introduced in [50] for projecting 6D and 5D representations onto $SO(3)$. 6D is equivalent to $\mathrm{GS}^+(M)$ (Eq. 9), and 5D utilizes a stereographic projection. **Spherical Regression** [22] (S^2**-Reg**) combines regression to the absolute values of a unit quaternion with classification of the signs. **3D-RCNN** [20] combines likelihood estimation and regression for predicting Euler angles. **Geodesic-Bin-and-Delta** (**M**$_G$ [25]) presents a hybrid model which combines classification over quantized pose space with regression of offsets from the quantized poses. **Quaternion**, **Euler angles**, and **axis-angle** are the classic parameterizations. In each case they are converted to matrix form before the loss is applied as in [50].

For SVD, 6D, 5D, and the classic representations, the loss is $L(R, R_t) = \frac{1}{2}\|R - R_t\|_F^2$. When $R, R_t \in SO(3)$ this is related to geodesic angle error θ as $L(R, R_t) = 2 - 2\cos(\theta)$. All other methods require an additional classification loss. See Appendix D for additional experimental details (architectures, implementations, etc).

4.1 3D point cloud alignment

The first experiment is the point cloud alignment benchmark from [50]. Given two shape point clouds the network is asked to predict the 3D rotation that best aligns them. The rotations in the dataset are sampled uniformly from $SO(3)$ (no rotation bias in the data).Table 1 (left) shows geodesic error statistics (mean, median, std) on the test set. We omit the maximum error as it is approx. $180°$ for all methods, a reflection of the symmetries in the data rather than limitations of the methods. SVD-Train outperforms all the baselines, and even SVD-Inference performs on par with the best baseline (6D). Interestingly, the hybrid approaches 3D-RCNN and M_G underperform the top regression baselines, a point we will return to later. Table 1 (middle) shows the mean errors on the test set as training progresses. The best performing methods at the end of training (SVD variations, and 6D) also show fast convergence. The errors at different percentiles are shown in Table 1 (right).

4.2 3D Pose estimation from 2D images

The second experiment follows the benchmark set forth in [22]. Images are rendered from Model-Net10 [45] objects from arbitrary viewpoints. Given a 2D image, the network must predict the object orientation. We used MobileNet [14] to generate image features, followed by fully connected regression layers. Rather than averaging over all 10 ModelNet categories as in [22], we focus on *chair* and *sofa* which are the two categories which exhibit the least rotational symmetries in the dataset. Results are shown in Tables 2 and 3. Interestingly, SVD-Inference also performs similarly to SVD-Train on final metrics with faster convergence, indicating short pretraining with SVD-Inference could improve convergence rates.

3D-RCNN and M_G are again underperforming the best methods. These hybrid methods have shown state of the art performance on predicting 3D pose from images [20, 25], but in those benchmarks the 3D rotations exhibit strong bias (camera viewpoints are not evenly distributed over $SO(3)$) which is

Table 2: **Pose estimation from ModelNet chair images.** We report the same metrics as in Table 1, see the caption there for a description. All models are trained for 550K steps in this case.

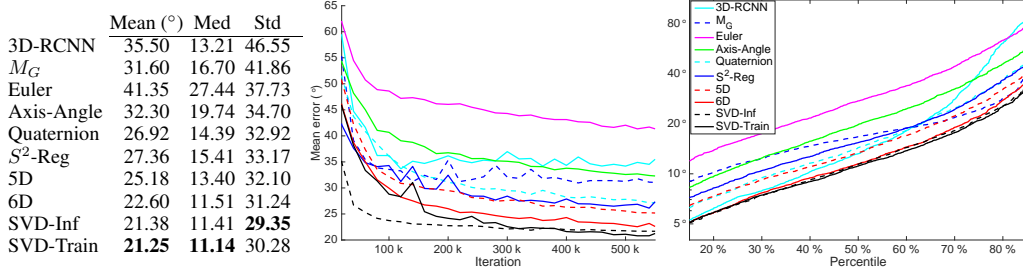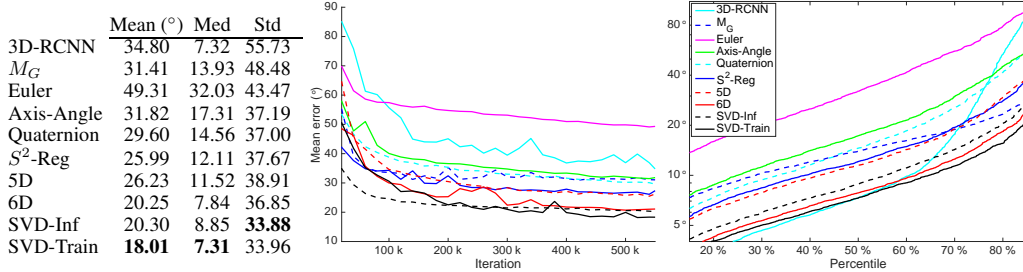|	Mean (°)	Med	Std
3D-RCNN	35.50	13.21	46.55
M_G	31.60	16.70	41.86
Euler	41.35	27.44	37.73
Axis-Angle	32.30	19.74	34.70
Quaternion	26.92	14.39	32.92
S^2-Reg	27.36	15.41	33.17
5D	25.18	13.40	32.10
6D	22.60	11.51	31.24
SVD-Inf	21.38	11.41	**29.35**
SVD-Train	**21.25**	**11.14**	30.28

Table 3: **Pose estimation from ModelNet sofa images.** We report the same metrics as in Table 1, see the caption there for a description. All models are trained for 550K steps in this case.

	Mean (°)	Med	Std
3D-RCNN	34.80	7.32	55.73
M_G	31.41	13.93	48.48
Euler	49.31	32.03	43.47
Axis-Angle	31.82	17.31	37.19
Quaternion	29.60	14.56	37.00
S^2-Reg	25.99	12.11	37.67
5D	26.23	11.52	38.91
6D	20.25	7.84	36.85
SVD-Inf	20.30	8.85	**33.88**
SVD-Train	**18.01**	**7.31**	33.96

a property their classification networks can exploit. In our experiments so far we have only considered rotations uniformly sampled from $SO(3)$.

4.3 Pascal 3D+

Pascal3D+ [46] is a standard benchmark for object pose estimation from single images. The dataset is composed of real images covering 12 categories. For training we discard occluded or truncated objects [25, 38] and augment with rendered images from [38]. The model architecture is the same as Section 4.2. Table 4 shows results on two categories and the mean over all categories (see Appendix D.7 for results on each of the 12 categories). The individual metrics we report are the median error as well as accuracies at $10°$, $15°$, and $20°$.

The best performing method is clearly S^2-Reg. As expected, the hybrid method 3D-RCNN performs well on this task, but SVD-Inference and SVD-Train are on par. The SVD variations are also the best performing of the regression methods (those that only train with a rotation loss). Interestingly, SVD-Inference slightly outperforms SVD-Train, which suggests in this scenario where viewpoints have a non-uniform prior, training a network to regress directly to the desired rotation can work well.

Table 4: **Pascal 3D+.** Accuracy at $10°$, $15°$, and $20°$ (higher is better), and median error are reported. On the left are results for *sofa* and *bicycle*. The third block is the results averaged over all 12 categories, and these numbers are used to determine the ranks shown on the right (lower is better).

	Sofa				Bicycle				Mean (12 categories)				Rank (12 categories)			
	Accuracy@			Med°	Accuracy@			Med°	Accuracy@			Med°	Accuracy@			Med°
	$10°$	$15°$	$20°$	Err	$10°$	$15°$	$20°$	Err	$10°$	$15°$	$20°$	Err	$10°$	$15°$	$20°$	Err
3D-RCNN	37.1	54.3	80.0	14.2	17.8	38.6	72.3	16.9	43.2	57.6	78.1	12.9	2	3	5	2
M_G	31.4	51.4	74.3	14.4	11.9	31.7	66.3	20.9	32.9	52.4	77.0	14.7	6	5	7	5
Euler	22.9	45.7	77.1	16.3	9.9	20.8	68.3	23.4	24.5	42.0	71.9	19.2	9	10	10	10
Axis-Angle	11.4	40.0	80.0	16.3	13.9	31.7	70.3	21.3	23.0	44.3	76.9	17.7	10	8	8	9
Quaternion	34.3	62.9	77.1	11.7	15.8	30.7	67.3	22.4	34.2	51.6	78.0	15.1	5	6	6	6
S^2-Reg	37.1	**65.7**	85.7	11.2	**21.8**	**45.5**	75.2	**16.1**	**45.8**	**64.4**	**83.8**	**11.3**	**1**	**1**	**1**	**1**
5D	17.1	54.3	77.1	14.2	10.9	26.7	68.3	21.1	25.2	43.9	75.6	17.0	8	9	9	8
6D	34.3	54.3	**88.6**	13.3	10.9	26.7	68.3	21.1	32.6	51.1	81.1	15.2	7	7	3	7
SVD-Inf	**45.7**	60.0	**88.6**	**11.0**	10.9	33.7	**84.2**	19.0	39.9	58.7	83.7	13.0	3	2	2	3
SVD-Train	40.0	57.1	85.7	12.7	9.9	26.7	80.2	20.9	35.1	52.7	80.5	14.6	4	4	4	4

Table 5: **Self-supervised 3D point cloud alignment.** The error metrics presented follow the same format as the earlier supervised point cloud alignment experiment, see Table 1. Although here the model is trained without rotation supervision, we show test errors in the predicted rotations. The legend on the right applies to both plots.
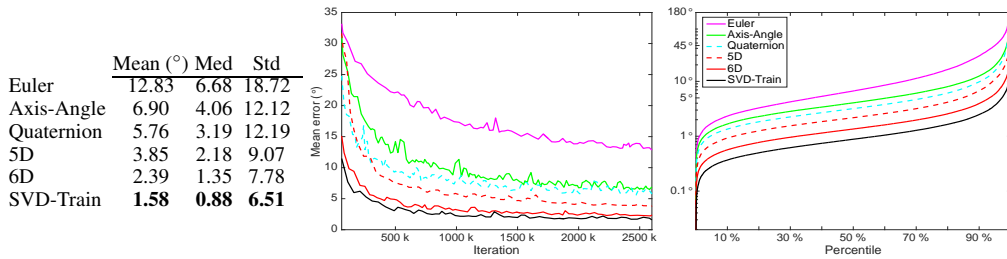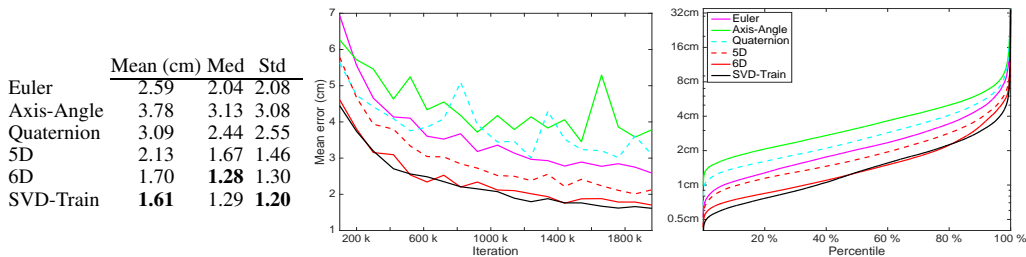
	Mean (°)	Med	Std
Euler	12.83	6.68	18.72
Axis-Angle	6.90	4.06	12.12
Quaternion	5.76	3.19	12.19
5D	3.85	2.18	9.07
6D	2.39	1.35	7.78
SVD-Train	**1.58**	**0.88**	**6.51**

Table 6: **Human pose inverse kinematics**. Following [50], we show errors in predicted joint locations in cm. As above, we show the test errors after training (left), mean errors while training progresses (middle), and percentiles on the right.

	Mean (cm)	Med	Std
Euler	2.59	2.04	2.08
Axis-Angle	3.78	3.13	3.08
Quaternion	3.09	2.44	2.55
5D	2.13	1.67	1.46
6D	1.70	**1.28**	1.30
SVD-Train	**1.61**	1.29	**1.20**

4.4 Unsupervised rotations

So far we have considered supervised rotation estimation. Given the growing attention to self- or unsupervised 3D learning [48, 26, 19, 50], it is important to understand how different representations fare without direct rotation supervision. We omit 3D-RCNN, M_G, and S^2-Reg from the experiments below as they require explicit supervision of classification terms, as well as SVD-Inference as it does not produce outputs on $SO(3)$ while training.

4.4.1 Self-supervised 3D point cloud alignment

To begin, we devise a simple variation of the point cloud alignment experiment from Section 4.1. Given two point clouds, the network still predicts the relative rotation. However, now the only loss is L2 on the point cloud registration after applying the predicted rotation. All other experiment details remain the same. From Table 5, SVD-Train performs significantly better than the next closest baseline, 6D.

4.4.2 Inverse kinematics

Our second unsupervised experiment is the human pose inverse kinematics experiment presented in [50]. A network is given 3D joint positions and is asked to predict the rotations from a canonical "T-pose" to the input pose. Predicted rotations are transformed back to joint positions via forward kinematics, and the training loss is on the reconstructed joint positions. We use the code provided by [50]. Table 6 presents the results. SVD-Train shows the best overall performance while 6D is closer than in other experiments.

4.4.3 Unsupervised depth estimation

The final experiment considers self-supervised learning of depth and ego-motion from videos [48]. Given a target image and source images, the model predicts a depth map for the target and camera poses from the target to sources. Source images are warped to the target view using predicted poses, and reconstruction loss on the warped image supervises training. In [48] the rotational component is parameterized by Euler angles. Following [48], we report the single-view depth estimation results

Table 7: **Single view depth estimation on KITTI.** We report the same metrics as in [48]. See Sec. 4.4.3.

	Error metric ↓				Accuracy metric ↑		
	Abs Rel	Sq Rel	RMSE	RMSE log	$\delta < 1.25$	$\delta < 1.25^2$	$\delta < 1.25^3$
Euler	0.216	3.163	7.169	0.291	0.720	0.893	0.952
Axis-Angle	**0.208**	2.752	7.099	0.287	**0.723**	0.894	**0.954**
Quaternion	0.218	3.055	7.251	0.294	0.707	0.888	0.950
5D	0.234	4.366	7.471	0.303	0.717	0.890	0.950
6D	0.217	3.103	7.320	0.297	0.716	0.891	0.951
SVD-Train	0.209	**2.517**	**7.045**	**0.286**	0.715	**0.895**	0.953

on KITTI [6] after 200K steps (Table 7). The error metrics are in meters while accuracy metrics are percentages up to a distance threshold in meters (see [4] for a description).

Observe that the difference between the best and second best method in each metric is small. This is not surprising since the camera pose is a small (albeit important) part of a complex deep architecture. Nonetheless, SVD-Train performs best for 4 out of the 7 metrics, and second best in another two. For driving data the motion is likely to be mostly planar for which axis-angle is well suited. Finally, it is worth noting that carefully selecting the rotation representation is important even in more complex models – the default selection of Euler angles in [48] is outperformed in every metric.

5 Conclusion

The results of the previous sections are broad and conclusive: a continuous 9D unconstrained representation followed by an SVD projection onto $SO(3)$ is consistently an effective, and often the state-of-the-art, representation for 3D rotations in neural networks. It is usable in a variety of application settings including without supervision. The strong empirical evidence is supported by a theoretical analysis that supports SVD as the preferred projection onto $SO(3)$.

References

[1] Martín Abadi, Ashish Agarwal, Paul Barham, Eugene Brevdo, Zhifeng Chen, Craig Citro, Greg S. Corrado, Andy Davis, Jeffrey Dean, Matthieu Devin, Sanjay Ghemawat, Ian Goodfellow, Andrew Harp, Geoffrey Irving, Michael Isard, Yangqing Jia, Rafal Jozefowicz, Lukasz Kaiser, Manjunath Kudlur, Josh Levenberg, Dan Mané, Rajat Monga, Sherry Moore, Derek Murray, Chris Olah, Mike Schuster, Jonathon Shlens, Benoit Steiner, Ilya Sutskever, Kunal Talwar, Paul Tucker, Vincent Vanhoucke, Vijay Vasudevan, Fernanda Viégas, Oriol Vinyals, Pete Warden, Martin Wattenberg, Martin Wicke, Yuan Yu, and Xiaoqiang Zheng. TensorFlow: Large-scale machine learning on heterogeneous systems, 2015. Software available from tensorflow.org.

[2] K. S. Arun, T. S. Huang, and S. D. Blostein. Least-squares fitting of two 3-D point sets. *IEEE Transactions on Pattern Analysis and Machine Intelligence*, 9(5):698–700, 1987.

[3] Zheng Dang, Kwang Moo Yi, Yinlin Hu, Fei Wang, Pascal Fua, and Mathieu Salzmann. Eigendecomposition-free training of deep networks with zero eigenvalue-based losses. In *European Conference on Computer Vision (ECCV)*, 2018.

[4] David Eigen, Christian Puhrsch, and Rob Fergus. Depth map prediction from a single image using a multi-scale deep network. In Z. Ghahramani, M. Welling, C. Cortes, N. D. Lawrence, and K. Q. Weinberger, editors, *Advances in Neural Information Processing Systems 27*, pages 2366–2374. Curran Associates, Inc., 2014.

[5] Sovann En, Alexis Lechervy, and Frédéric Jurie. Rpnet: An end-to-end network for relative camera pose estimation. In *European Conference on Computer Vision Workshops (ECCVW)*, 2018.

[6] Andreas Geiger, Philip Lenz, and Raquel Urtasun. Are we ready for autonomous driving? the KITTI vision benchmark suite. In *IEEE Conference on Computer Vision and Pattern Recognition (CVPR)*, pages 3354–3361, 2012.

[7] Mike B. Giles. Collected matrix derivative results for forward and reverse mode algorithmic differentiation. In Christian H. Bischof, H. Martin Bücker, Paul D. Hovland, Uwe Naumann, and J. Utke, editors, *Advances in Automatic Differentiation*, pages 35–44. Springer, 2008.

[8] Igor Gilitschenski, Roshni Sahoo, Wilko Schwarting, Alexander Amini, Sertac Karaman, and Daniela Rus. Deep orientation uncertainty learning based on a bingham loss. In *International Conference on Learning Representations (ICLR)*, 2020.

[9] Gene H. Golub and Charles F. Van Loan. *Matrix Computations (3rd Ed.)*. Johns Hopkins University Press, Baltimore, MD, USA, 1996.

[10] A.K. Gupta and D.K. Nagar. *Matrix Variate Distributions*. Monographs and Surveys in Pure and Applied Mathematics. Taylor & Francis, 1999.

[11] Richard Hartley, Jochen Trumpf, Yuchao Dai, and Hongdong Li. Rotation averaging. *International Journal of Computer Vision*, 101(2), 2013.

[12] Richard Hartley and Andrew Zisserman. *Multiple View Geometry in Computer Vision*. Cambridge University Press, New York, NY, USA, 2nd edition, 2003.

[13] Berthold K. P. Horn, Hugh M. Hilden, and Shahriar Negahdaripour. Closed-form solution of absolute orientation using orthonormal matrices. *J. Opt. Soc. Am. A*, 5(7):1127–1135, Jul 1988.

[14] Andrew G. Howard, Menglong Zhu, Bo Chen, Dmitry Kalenichenko, Weijun Wang, Tobias Weyand, Marco Andreetto, and Hartwig Adam. MobileNets: Efficient convolutional neural networks for mobile vision applications. *CoRR*, abs/1704.04861, 2017.

[15] Lei Huang, Dawei Yang, Bo Lang, and Jia Deng. Decorrelated batch normalization. In *IEEE Conference on Computer Vision and Pattern Recognition (CVPR)*, June 2018.

[16] Catalin Ionescu, Orestis Vantzos, and Cristian Sminchisescu. Training deep networks with structured layers by matrix backpropagation. *CoRR*, abs/1509.07838, 2015.

[17] Kui Jia, Shuai Li, Yuxin Wen, Tongliang Liu, and Dacheng Tao. Orthogonal deep neural networks. *CoRR*, abs/1905.05929, 2019.

[18] Wolfgang Kabsch. A solution for the best rotation to relate two sets of vectors. *Acta Crystallographica Section A: Crystal Physics, Diffraction, Theoretical and General Crystallography*, 32(5):922–923, 1976.

[19] Angjoo Kanazawa, Michael J. Black, David W. Jacobs, and Jitendra Malik. End-to-end recovery of human shape and pose. In *IEEE Conference on Computer Vision and Pattern Recognition (CVPR)*, 2018.

[20] A. Kundu, Y. Li, and J. M. Rehg. 3D-RCNN: Instance-level 3D object reconstruction via render-and-compare. In *IEEE Conference on Computer Vision and Pattern Recognition (CVPR)*, pages 3559–3568, 2018.

[21] Yi Li, Gu Wang, Xiangyang Ji, Yu Xiang, and Dieter Fox. DeepIM: Deep iterative matching for 6D pose estimation. In *The European Conference on Computer Vision (ECCV)*, September 2018.

[22] Shuai Liao, Efstratios Gavves, and Cees G. M. Snoek. Spherical regression: Learning viewpoints, surface normals and 3d rotations on n-spheres. In *IEEE Conference on Computer Vision and Pattern Recognition (CVPR)*, 2019.

[23] Per-Olov Löwdin. On the nonorthogonality problem. *Advances in Quantum Chemistry*, 5:185–199, 1970.

[24] Siddharth Mahendran, Haider Ali, and René Vidal. 3d pose regression using convolutional neural networks. In *IEEE Conference on Computer Vision and Pattern Recognition Workshops (CVPRW)*, 2017.

[25] Siddharth Mahendran, Haider Ali, and René Vidal. A mixed classification-regression framework for 3D pose estimation from 2D images. In *British Machine Vision Conference (BMVC)*, 2018.

[26] Reza Mahjourian, Martin Wicke, and Anelia Angelova. Unsupervised learning of depth and ego-motion from monocular video using 3D geometric constraints. In *The IEEE Conference on Computer Vision and Pattern Recognition (CVPR)*, 2018.

[27] Iaroslav Melekhov, Juha Ylioinas, Juho Kannala, and Esa Rahtu. Relative camera pose estimation using convolutional neural networks. In *International Conference on Advanced Concepts for Intelligent Vision Systems*, 2017.

[28] Takeru Miyato, Toshiki Kataoka, Masanori Koyama, and Yuichi Yoshida. Spectral normalization for generative adversarial networks. In *International Conference on Learning Representations*, 2018.

[29] Arsalan Mousavian, Dragomir Anguelov, John Flynn, and Jana Kosecka. 3d bounding box estimation using deep learning and geometry. In *The IEEE Conference on Computer Vision and Pattern Recognition (CVPR)*, 2017.

[30] Théodore Papadopoulo and Manolis I. A. Lourakis. Estimating the jacobian of the singular value decomposition: Theory and applications. In *Computer Vision - ECCV 2000*, pages 554–570. Springer Berlin Heidelberg, 2000.

[31] Adam Paszke, Sam Gross, Francisco Massa, Adam Lerer, James Bradbury, Gregory Chanan, Trevor Killeen, Zeming Lin, Natalia Gimelshein, Luca Antiga, Alban Desmaison, Andreas Kopf, Edward Yang, Zachary DeVito, Martin Raison, Alykhan Tejani, Sasank Chilamkurthy, Benoit Steiner, Lu Fang, Junjie Bai, and Soumith Chintala. Pytorch: An imperative style, high-performance deep learning library. In H. Wallach, H. Larochelle, A. Beygelzimer, F. dAlche Buc, E. Fox, and R. Garnett, editors, *Advances in Neural Information Processing Systems 32*, pages 8024–8035. Curran Associates, Inc., 2019.

[32] Omid Poursaeed, Guandao Yang, Aditya Prakash, Qiuren Fang, Hanqing Jiang, Bharath Hariharan, and Serge Belongie. Deep fundamental matrix estimation without correspondences. In *European Conference on Computer Vision*, pages 485–497, 2018.

[33] Thomas Probst, Danda Pani Paudel, Ajad Chhatkuli, and Luc Van Gool. Unsupervised learning of consensus maximization for 3d vision problems. In *IEEE Conference on Computer Vision and Pattern Recognition (CVPR)*, June 2019.

[34] Sergey Prokudin, Peter Gehler, and Sebastian Nowozin. Deep directional statistics: Pose estimation with uncertainty quantification. In *European Conference on Computer Vision (ECCV)*, September 2018.

[35] P.H. Schönemann. A generalized solution of the orthogonal procrustes problem. *Psychometrika*, 31:1–10, 1966.

[36] Karen Simonyan and Andrew Zisserman. Very deep convolutional networks for large-scale image recognition. In *International Conference on Learning Representations (ICLR)*, 2015.

[37] John Stuelpnagel. On the parametrization of the three-dimensional rotation group. *SIAM Review*, 6(4):422–430, 1964.

[38] Hao Su, Charles R. Qi, Yangyan Li, and Leonidas J. Guibas. Render for cnn: Viewpoint estimation in images using cnns trained with rendered 3d model views. In *The IEEE International Conference on Computer Vision (ICCV)*, December 2015.

[39] Martin Sundermeyer, Zoltan-Csaba Marton, Maximilian Durner, Manuel Brucker, and Rudolph Triebel. Implicit 3d orientation learning for 6d object detection from rgb images. In *The European Conference on Computer Vision (ECCV)*, September 2018.

[40] Supasorn Suwajanakorn, Noah Snavely, Jonathan J. Tompson, and Mohammad Norouzi. Discovery of latent 3d keypoints via end-to-end geometric reasoning. In *Advances in Neural Information Processing Systems (NIPS)*, pages 2063–2074, 2018.

[41] Camillo J. Taylor and David J. Kriegman. Minimization on the Lie group SO(3) and related manifolds. Technical report, Yale University, 1994.

[42] James Townsend. Differentiating the singular value decomposition, August 2016.

[43] Shubham Tulsiani and Jitendra Malik. Viewpoints and keypoints. In *IEEE Conference on Computer Vision and Pattern Recognition (CVPR)*, 2015.

[44] Grace Wahba. A least squares estimate of satellite attitude. *SIAM Review*, 7(3):409–409, 1965.

[45] Zhirong Wu, Shuran Song, Aditya Khosla, Fisher Yu, Linguang Zhang, Xiaoou Tang, and Jianxiong Xiao. 3D shapeNets: A deep representation for volumetric shapes. In *IEEE Conference on Computer Vision and Pattern Recognition (CVPR)*, June 2015.

[46] Yu Xiang, Roozbeh Mottaghi, and Silvio Savarese. Beyond PASCAL: A benchmark for 3d object detection in the wild. In *2014 IEEE Winter Conference on Applications of Computer Vision (WACV)*, pages 75–82, March 2014.

[47] Yu Xiang, Tanner Schmidt, Venkatraman Narayanan, and Dieter Fox. PoseCNN: A convolutional neural network for 6D object pose estimation in cluttered scenes. *Robotics: Science and Systems (RSS)*, 2018.

[48] Tinghui Zhou, Matthew Brown, Noah Snavely, and David G. Lowe. Unsupervised learning of depth and ego-motion from video. In *IEEE Conference on Computer Vision and Pattern Recognition (CVPR)*, 2017.

[49] Xingyi Zhou, Xiao Sun, Wei Zhang, Shuang Liang, and Yichen Wei. Deep kinematic pose regression. In *European Conference on Computer Vision Workshops (ECCVW)*, 2016.

[50] Yi Zhou, Connelly Barnes, Jingwan Lu, Jimei Yang, and Hao Li. On the continuity of rotation representations in neural networks. In *The IEEE Conference on Computer Vision and Pattern Recognition (CVPR)*, June 2019.

A Complete proof of Proposition 1

In the main paper, we gave the derivative of the orthogonalization operators $\texttt{SVDO}(M)$ and $\texttt{GS}(M)$ and the resulting error under Gaussian noise, near the identity matrix $M = I$. We now give the complete proof and discussion of Proposition 1 and the additional facts about smoothness of $\texttt{SVDO}(M), \texttt{SVDO}^+(M)$.

Note that since $\texttt{SVDO}(RM) = R \cdot \texttt{SVDO}(M)$ and $\texttt{GS}(RM) = R \cdot \texttt{GS}(M)$ for any orthogonal matrix R, and likewise for $\texttt{SVDO}^+, \texttt{GS}^+$ if R is *special* orthogonal. Therefore the error analyses are the same for all matrices M:

$$\|\texttt{GS}(R + \sigma N) - R\|_F^2 = \|R(\texttt{GS}(I + \sigma R^{-1}N) - I)\|_F^2 = \|\texttt{GS}(I + \sigma N) - I\|_F^2 \qquad (15)$$

since orthogonal matrices preserve Frobenius norm and $R^{-1}N$ has the same distribution as N since N was assumed isotropic. (The same applies for the other three functions.)

Proof of Proposition 1. (1) Let M have SVD $M = U\Sigma V^T$ for some orthogonal matrices U, V and diagonal matrix $\Sigma \geq 0$. To first order in σ, we can expand each of U, Σ, V^T as

$$U = U_0(I + \sigma U_1), \qquad (16)$$
$$\Sigma = \Sigma_0 + \sigma\Sigma_1, \qquad (17)$$
$$V = V_0(I + \sigma V_1), \qquad (18)$$

with U_0, V_0 orthogonal, U_1, V_1 antisymmetric and $\Sigma_0, \Sigma_1 \geq 0$ diagonal. This is using the fact that the antisymmetric matrices give the tangent space to the orthogonal matrices. Similarly, the tangent space to the diagonal matrices is given again by the diagonal matrices. This gives an overall expression for M as

$$M = I + \sigma N = U_0(I + \sigma U_1)(\Sigma_0 + \sigma\Sigma_1)(I + \sigma V_1)^T V_0^T. \qquad (19)$$

Setting $\sigma = 0$ we see $I = U_0\Sigma_0 V_0^T$, which implies $\Sigma_0 = I$ and $U_0 = V_0$. Next, collecting the first-order σ terms gives

$$N = U_0(U_1 + \Sigma_1 + V_1^T)U_0^T. \qquad (20)$$

If a matrix X is (anti-)symmetric and Q is orthogonal, then QXQ^T is again (anti-)symmetric. So, the symmetric and antisymmetric parts of the equation are

$$S = U_0\Sigma_1 U_0^T, \quad A = U_0(U_1 + V_1^T)U_0^T. \qquad (21)$$

Note that the first equation is an SVD of the symmetric part of N, while the second equation shows that U_1 and V_1 satisfy $U_1 + V_1^T = U_0^T A U_0$. Finally, dropping the $\Sigma_0 + \sigma\Sigma_1$ factor from Eq. (19) and expanding out shows that $\texttt{SVDO}(I + \sigma N) = I + \sigma A + O(\sigma^2)$.

(2) Let $M = QR$, where Q is orthogonal and R is upper-triangular with positive diagonal. As above, by expanding to first order in σ we have

$$I + \sigma N = Q_0(I + \sigma Q_1)(I + \sigma R_1)R_0, \qquad (22)$$

with Q_0 orthogonal, Q_1 antisymmetric, and R_1, R_0 upper triangular. Setting $\sigma = 0$, we see $I = Q_0 R_0$ and so $Q_0 = R_0 = I$. For the σ terms, we split N into its upper, lower and diagonal parts to get

$$U + D + L = Q_1 + R_1, \tag{23}$$

which by comparing parts gives $Q_1 = L - L^T$ and $R_1 = U + D + L^T$. Then $\mathtt{GS}(M) = I + \sigma(L - L^T)$ by simple algebra.

We now prove Corollary 1.

Corollary 1 (restated). If N is 3×3 with i.i.d. Gaussian entries $n_{ij} \sim \mathcal{N}(0, 1)$, then with error of order $O(\sigma^3)$,

$$\mathbb{E}[\|\mathtt{SVDO}(M) - I\|_F^2] = 3\sigma^2, \qquad \mathbb{E}[\|\mathtt{GS}(M) - I\|_F^2] = 6\sigma^2 \tag{24}$$

$$\mathbb{E}[\|\mathtt{SVDO}(M) - M\|_F^2] = 6\sigma^2, \qquad \mathbb{E}[\|\mathtt{GS}(M) - M\|_F^2] = 9\sigma^2 \tag{25}$$

Proof. Simplifying the error expressions using the first-order calculations in the Proposition gives

$$\|\mathtt{SVDO}(M) - I\|_F^2 \;=\; \|\sigma A\|_F^2, \tag{26}$$

$$\|\mathtt{GS}(M) - I\|_F^2 \;=\; \|\sigma(L - L^T)\|_F^2, \tag{27}$$

$$\|\mathtt{SVDO}(M) - M\|_F^2 \;=\; \|-\sigma S\|_F^2, \tag{28}$$

$$\|\mathtt{GS}(M) - M\|_F^2 \;=\; \|-\sigma(U + D + L^T)\|_F^2, \tag{29}$$

with notation for S, A, U, D, L as in the proposition. Thus each expression is σ^2 times the Frobenius norm of the corresponding matrix. Each entry of $A, L - L^T, S$ and $U + D + L^T$ is a linear combination of the entries of N, hence is Gaussian since N has i.i.d. Gaussian entries $n_{ij} \sim \mathcal{N}(0, 1)$. The expectations are the sums of the entrywise expectations of these matrices. For example, $A = \frac{1}{2}(N - N^T)$ has six nonzero entries of the form $\frac{1}{2}(n_{ij} - n_{ji})$, each having variance $\frac{1}{2}$, so $\mathbb{E}[\|A\|_F^2] = 3$. For $L - L^T$, the above diagonal entries are $-n_{ji}$ and the below-diagonal entries are n_{ij}, and the diagonal is 0, so the total variance is 6. The other two calculations are similar (the entries do not all have the same variances).

Remark. The tangent space to the identity matrix along the orthogonal matrices is the space of antisymmetric matrices. Both of the calculations above can be thought of as giving orthogonal approximations of the form

$$I + \sigma N \approx I + \sigma A', \tag{30}$$

where A' is a choice of antisymmetric matrix that depends on the approximation method. The fact that $\mathtt{SVDO}(M)$ produces the approximation $A' = A = \frac{1}{2}(N - N^T)$ means it corresponds to the natural projection of N onto the orthogonal tangent space. By contrast, $\mathtt{GS}(M)$ produces $A' = L - L^T$, essentially a "greedy" choice with respect to the starting matrix (minimizing the change to the leftmost columns). For certain matrices $\mathtt{GS}$ can have smaller error: for example if N happens to be upper-triangular, $\mathtt{GS}(M) = I$ and the error is zero. For isotropic noise, however, the SVD approximation is the most efficient in expectation.

A.1 Accuracy of error estimates as σ increases

From Corollary 1 (Sec 3.3) we see special-orthogonalization with Gram-Schmidt ($\mathtt{GS}^+$) produces twice the error in expectation as SVD ($\mathtt{SVDO}^+$) for $SO(3)$ reconstruction when inputs are perturbed by Gaussian noise. We compare these derived errors with numerical simulations. See Figure 1.

B Proof of smoothness and discussion

Proposition 2 *The symmetric orthogonalization $\mathtt{SVDO}(M)$ is a smooth function of M if $\det(M) \neq 0$.*

Proof. We use the Implicit Function Theorem and the least-squares characterization of $\mathtt{SVDO}(M)$ as

$$\mathtt{SVDO}(M) = \underset{Q \in O(n)}{\arg\min} \|M - Q\|_F^2. \tag{31}$$
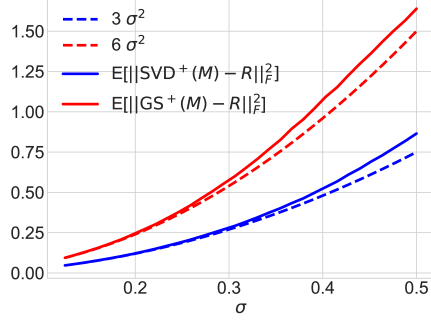
Figure 1: **Simulations.** We plot our derived approximations against numerical simulations of the expected error in reconstruction under additive noise. For each σ we compute the numerical expectation with 100K trials. These plots can provide a sanity check of our derivations.

We calculate the derivative with respect to $Q \in O(n)$: for A an antisymmetric matrix,

$$\lim_{\epsilon \to 0} \tfrac{1}{\epsilon}(\|M - Q(I + \epsilon A)\|_F^2 - \|M - Q\|_F^2) = -2\operatorname{Tr}(M^T Q A). \tag{32}$$

If this vanishes for every A, then $M^T Q$ is symmetric, that is, (M, Q) is a root of the function $g(M, Q) = M^T Q - Q^T M$. Let M_0 be a fixed matrix. As discussed above, the optimal solution to this equation is given by an SVD, $M_0 = U_0 S_0 V_0^T$, yielding $Q_0 = U_0 V_0^T$. To show that Q is a smooth function of M, it suffices by the Implicit Function Theorem to show that the Jacobian matrix $\frac{\partial g}{\partial Q}$ is full-rank at (M_0, Q_0). To see this, we differentiate it again:

$$\frac{\partial g}{\partial Q}(A) = \lim_{\epsilon \to 0} \frac{1}{\epsilon}(g(M_0, Q_0(I + \epsilon A)) - g(M_0, Q_0)) = M_0^T Q_0 A - A^T Q_0^T M_0, \tag{33}$$

where A is antisymmetric. Some algebra shows that this is, equivalently,

$$\frac{\partial g}{\partial Q}(A) = V_0(S_0 V_0^T A V_0 + V_0^T A V_0 S_0)V_0^T. \tag{34}$$

To see that this is an invertible transformation of A, note that conjugating by V_0 is invertible since V_0 is orthogonal. So it is equivalent to show that the function

$$A \mapsto S_0 A + A S_0 \tag{35}$$

is invertible. This function just rescales the entry a_{ij} to $(s_i + s_j)a_{ij}$. Since the singular values are positive this is invertible as desired.

Proposition 3 *The special symmetric orthogonalization is a smooth function of M if either of the following is true:*

- $\det(M) > 0$,

- $\det(M) < 0$ *and the smallest singular value of M has multiplicity one.*

Proof sketch. The analysis is identical to the main proof, except that if $\det(M) < 0$, S_0 is effectively altered so that the last entry is changed from s_n to $-s_n$. Thus the function $A \mapsto S_0 A + A S_0$ now sends the entry a_{ij} to $(\pm s_i \pm s_j)a_{ij}$, with negative signs at $i = n$ and/or $j = n$. If s_n occurred with multiplicity one, the result is still invertible since $s_i - s_n \neq 0$ for $i \neq n$ and for $i = j = n$ the coefficient is $-2s_n$. Otherwise, however, $s_{n-1} = s_n$ and the operation sends $a_{n-1,n}$ to $(s_{n-1} - s_n)a_{n-1,n} = 0$; likewise for $a_{n,n-1}$. In this case there are many optimal *special* orthogonalizations of M_0, and the operation is not even continuous in a neighborhood of M_0.

14

C   Gradients

Here we provide the detailed derivation sketched out in Sec 3.2. We will first analyze $\frac{\partial L}{\partial M}$ for $\texttt{SVDO}(M)$. With $\circ$ denoting the Hadamard product, from [16, 42] we have

$$\frac{\partial L}{\partial M} \quad = \quad U[(F \circ (U^T \frac{\partial L}{\partial U} - \frac{\partial L}{\partial U}^T U))\Sigma + \Sigma(F \circ (V^T \frac{\partial L}{\partial V} - \frac{\partial L}{\partial V}^T V))]V^T, \qquad (36)$$

$$F_{i,j} \quad = \quad \begin{cases} \frac{1}{s_i^2 - s_j^2}, & \text{if } i \neq j \\ 0, & \text{if } i = j \end{cases}, \quad s_i = \Sigma_{ii}. \qquad (37)$$

Letting $X = U^T \frac{\partial L}{\partial U} - \frac{\partial L}{\partial U}^T U$, and $Y = V^T \frac{\partial L}{\partial V} - \frac{\partial L}{\partial V}^T V$, we see that X, Y are antisymmetric. Furthermore, since $\|\texttt{SVDO}(M) - R\|_F^2 = 2\operatorname{Tr}(\mathbb{I}_n) - 2\operatorname{Tr}(UV^T R^T)$, then $\frac{\partial L}{\partial U} = -2RV$, and $\frac{\partial L}{\partial V} = -2R^T U$. This leads directly to $X = Y^T = -Y$. We can simplify Eq. 36 as

$$\frac{\partial L}{\partial M} \quad = \quad U((F \circ X)\Sigma - \Sigma(F \circ X))V^T. \qquad (38)$$

Inspecting the individual elements of $(F \circ X)\Sigma$ and $\Sigma(F \circ X))$ we have

$$((F \circ X)\Sigma)_{ij} = \frac{X_{ij}s_j}{s_i^2 - s_j^2}, \qquad (\Sigma(F \circ X))_{ij} = \frac{X_{ij}s_i}{s_i^2 - s_j^2}. \qquad (39)$$

Letting $Z = (F \circ X)\Sigma - \Sigma(F \circ X)$, we can simplify $\frac{\partial L}{\partial M} = UZV^T$ where the elements of Z are

$$Z_{ij} \quad = \quad \begin{cases} \frac{-X_{ij}}{s_i + s_j}, & \text{if } i \neq j \\ 0, & \text{if } i = j. \end{cases} \qquad (40)$$

For $\texttt{SVDO}(M)$ Eq. 40 tells us $\frac{\partial L}{\partial M}$ is undefined whenever two singular values are both zero and large when their sum is very near zero.

For $\texttt{SVDO}^+(M)$, if $\det(M) > 0$ then the analysis is the same as above. If $\det(M) < 0$, the extra factor $D = \operatorname{diag}(1, 1, \ldots, -1)$ effectively changes the smallest singular value s_n to $-s_n$. The derivation is otherwise unchanged. In particular the denominator in equation (40) is now $s_j - s_n$ or $s_n - s_i$ if either i or j is n.

C.1   Gradients observed during training

In Figure 2 (left) we see the gradient norms observed while training for point cloud alignment (Section 4.1). SVD-Train has the same profile as for 6D ($\texttt{GS}^+$). SVD-Train converges quickly (relative to all other methods) in all of our experiments, indicating no instabilities due to large gradients.

On the right of Figure 2 we profile the gradients for the scenario where we begin training with the SVD-Inference loss and switch to SVD-Train after 100K steps (after roughly 4% of training iterations). SVD-Inf trains the network to produce outputs that are close to $SO(3)$, which eliminates some conditions of instability in Eq. 40. This is confirmed by seeing much smaller gradient norms after switching to SVD-Train at 100K steps. Note, this approach was never used (or needed) in our experiments.

D   Experiments

D.1   Additional baseline implementation details

- **6D** is the partial Gram-Schmidt method which computes $\texttt{GS}^+(M)$. Our implementation follows exactly the code provided by [50].
- **5D** maps outputs in $\mathbb{R}^5$ onto $SO(3)$ as described in [50].
- **Spherical Regression** (S^2-**Reg**) regresses to n-spheres. Following [22], we use regression to S^1 for Pascal3D+ and S^3 regression (quaternions) for their ModelNet experiments (section 4.2). The method combines abs. value regression with sign classification. Our implementation of the final regression layers follows the provided code. We select the hyperparameter that balances the classification and regression losses by a simple line search in the neighborhood of the default provided in [22].
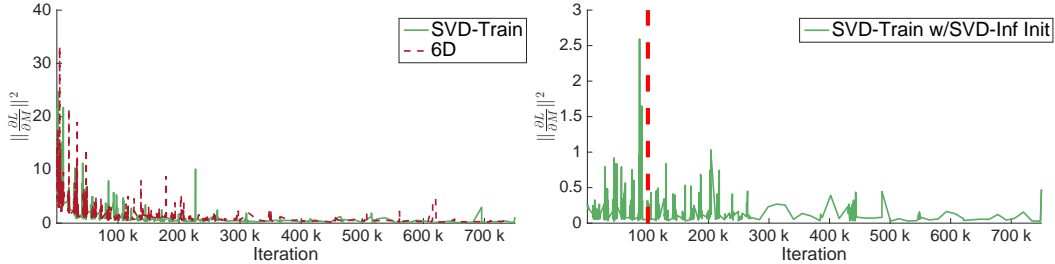
Figure 2: **Gradients.** Left are the gradient norms $\|\frac{\partial L}{\partial M}\|_F^2$ for the point cloud alignment experiment. SVD-Train and 6D have similar profiles. On the right the network is trained with SVD-Inf for the first 100K steps, then SVD-Train. During the first 100K steps the network learns to output matrices close to $SO(3)$ and this eliminates sources of high gradient norms in Eq. 40.

S^2-Reg uses both classification and regression losses, not surprisingly we were unable to train successfully on any of the unsupervised rotation experiments. The closest we came was on unsupervised point cloud alignment (Sec 4.4). With careful hyperparameter tuning the model completed training with mean test errors near $90°$.

- **3D-RCNN** [20] combines likelihood estimation and regression (via expectation) for predicting Euler angles. This representation also requires both classification and regression losses for training, and we were unable to make the model train successfully on the unsupervised rotation experiments.

- **Geodesic-Bin-and-Delta** (M_G [25]) combines classification over quantized pose space (axis-angle representation) with regression of offsets. For our experiments with where observed rotations are uniformly distributed over $SO(3)$ (Sec. 4.1, 4.2), K-means clustering is ineffective. Instead we quantize $SO(3)$ by uniformly sampling a large number (1000) of rotations (larger values did not improve results). We found this version of Geodesic-Bin-and-Delta outperformed the One-delta-network-per-pose-bin variation in these experiments. For Pascal3D+ we follow the reference and use K-means with $K = 200$. This method also requires both classification and regression losses and we were unable to train successfully in the unsupervised setting.

- **Quaternion**, **Euler angles**, and **axis-angle** are the classic parameterizations. In each case they are converted to matrix form before the loss is applied. In our experiments we did not filter any outputs from the network representing angles (e.g. clipping values or applying activations such as $\tanh$). We found this gave the best results overall.

D.2   Learning rate decay

An observation from the point cloud registration results is that the curves for mean test errors as training progresses do not decay smoothly as one might expect for any method (Table 1, middle, in the main paper). This is in part due to the training code from [50] does not utilize a learning rate decay for this experiment. It is reasonable to observe the variance in evaluation when a decay is introduced as would be common in practice. Table 8 (left) shows the curves when the learning rate is exponentially decayed (decay rate of 0.95, decay steps of 35K). The evaluation over time is smoother but the results are consistent with those presented in the main paper.

D.3   Geodesic loss

In [50] it was shown that geodesic loss for training did not alter the results much, and we have the same observation. Table 8 (right) shows the geodesic loss results.

D.4   Architecture details

D.4.1   3D point cloud alignment (Sec. 4.1)

The model architecture follows exactly the architecture described in [50]. Point clouds are embedded with simplified PointNet (4-layer MLP) ending with a global max-pooling. Three dense layers

Table 8: **Left: Training point cloud alignment with learning rate decay**. Evaluation is smoother over time but the comparative analysis does not change. **Right: geodesic loss.** Training with geodesic loss for point cloud alignment. Relative performances are consistent with squared Frobenius loss (Table 1 in main paper).
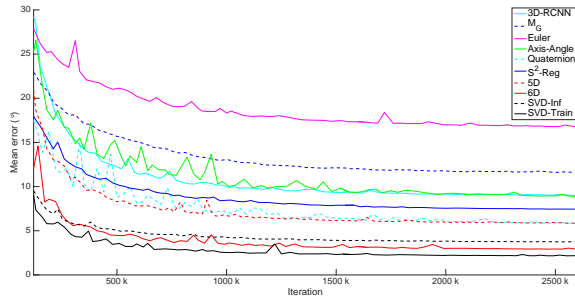
	Mean ($^\circ$)	Med	Std
5D	3.88	2.08	9.19
6D	2.29	1.30	7.52
SVD-Train	2.05	1.28	7.15

make up the regression network. The output dimensionality of the final layer depends on the chosen representation. For classification+regression models the final layers follows the relevant references.

D.4.2 3D Pose estimation from 2D images (Sec. 4.2), and Pascal3D+ (Sec. 4.3)

The regression layers are the same as above. The image embeddings are generated with MobileNet [14]. We found no difference in performance between MobileNet and VGG16 [36] (not surprising given the comparison in [14]).

D.5 Inverse kinematics (Sec. 4.4.2) and unsupervised depth estimation (Sec. 4.4.3)

For these experiments the training and evaluation code is provided by [50] and [48], respectively. We simply change the rotation representation layer.

D.6 Remark on timings

We noticed no measurable difference in training time with SVDO$^+$ as expected, since the forward and backward pass for small, e.g. 3×3, SVD is efficient.

D.7 Pascal3D+ full results.

Here in Table 9 we show the results for all 12 categories in the Pascal3D+.

Table 9: **Pascal 3D+.** Results for all 12 categories.

	aeroplane Accuracy@ 10°	15°	20°	Med° Err	bottle Accuracy@ 10°	15°	20°	Med° Err	chair Accuracy@ 10°	15°	20°	Med° Err	sofa Accuracy@ 10°	15°	20°	Med° Err
3D-RCNN	32.8	52.5	77.9	13.5	61.3	74.2	90.3	7.2	29.7	45.1	69.8	17.2	37.1	54.3	80.0	14.2
M_G	22.1	45.1	82.4	16.0	48.4	62.9	87.1	11.0	23.1	45.6	75.8	15.9	31.4	51.4	74.3	14.4
Euler	15.2	35.3	70.1	19.8	58.1	69.4	91.9	9.0	9.3	28.6	58.8	25.3	22.9	45.7	77.1	16.3
Axis-Angle	16.7	34.8	74.5	20.0	50.0	67.7	91.9	10.4	11.5	27.5	69.8	21.7	11.4	40.0	80.0	16.3
Quaternion	28.9	46.6	77.5	16.0	53.2	71.0	91.9	8.3	19.8	37.4	73.1	18.6	34.3	62.9	77.1	11.7
S^2-Reg	46.6	67.6	87.3	10.6	56.5	69.4	91.9	8.8	37.4	61.5	84.6	12.7	37.1	65.7	85.7	11.2
5D	21.6	38.7	75.5	17.3	54.8	66.1	93.5	9.2	17.6	34.6	72.0	19.1	17.1	54.3	77.1	14.2
6D	24.0	42.6	75.5	17.3	54.8	71.0	95.2	9.3	20.9	39.6	78.6	17.2	34.3	54.3	88.6	13.3
SVD-Inf	26.0	57.4	86.3	13.3	56.5	75.8	95.2	8.9	20.3	43.4	77.5	16.8	45.7	60.0	88.6	11.0
SVD-Train	22.1	43.6	77.0	17.4	53.2	75.8	93.5	7.7	24.2	39.0	71.4	17.6	40.0	57.1	85.7	12.7

	bicycle Accuracy@ 10°	15°	20°	Med° Err	bus Accuracy@ 10°	15°	20°	Med° Err	diningtable Accuracy@ 10°	15°	20°	Med° Err	train Accuracy@ 10°	15°	20°	Med° Err
3D-RCNN	17.8	38.6	72.3	16.9	88.7	91.5	93.7	4.4	46.7	60.0	66.7	12.2	65.7	74.7	82.8	6.4
M_G	11.9	31.7	66.3	20.9	76.1	88.0	95.1	7.6	26.7	53.3	60.0	12.8	48.5	66.7	82.8	10.1
Euler	9.9	20.8	68.3	23.4	47.2	66.9	87.3	10.5	26.7	40.0	73.3	16.6	42.4	63.6	80.8	11.1
Axis-Angle	13.9	31.7	70.3	21.3	38.7	69.7	93.7	12.0	26.7	53.3	80.0	14.4	40.4	64.6	82.8	11.6
Quaternion	15.8	30.7	67.3	22.4	69.7	83.8	92.3	7.4	33.3	46.7	73.3	17.3	56.6	68.7	81.8	8.7
S^2-Reg	21.8	45.5	75.2	16.1	93.7	98.6	99.3	3.8	33.3	46.7	66.7	15.3	66.7	76.8	84.8	6.2
5D	10.9	26.7	68.3	21.1	52.1	72.5	93.0	9.6	33.3	60.0	66.7	11.4	35.4	49.5	78.8	15.5
6D	14.9	27.7	71.3	22.0	66.9	83.8	94.4	7.9	13.3	46.7	73.3	15.3	63.6	73.7	80.8	7.7
SVD-Inf	10.9	33.7	84.2	19.0	80.3	92.3	95.8	6.1	53.3	60.0	73.3	10.0	58.6	73.7	82.8	8.5
SVD-Train	9.9	26.7	80.2	20.9	67.6	85.2	96.5	7.9	33.3	53.3	73.3	13.0	63.6	72.7	81.8	8.4

	boat Accuracy@ 10°	15°	20°	Med° Err	car Accuracy@ 10°	15°	20°	Med° Err	motorbike Accuracy@ 10°	15°	20°	Med° Err	tvmonitor Accuracy@ 10°	15°	20°	Med° Err
3D-RCNN	12.6	23.2	52.6	27.0	65.5	76.8	86.3	6.7	24.6	46.5	81.6	15.6	35.5	53.9	82.9	13.2
M_G	16.8	27.4	56.8	25.2	51.2	70.2	86.9	9.8	15.8	40.4	79.8	17.1	23.0	46.1	77.0	15.9
Euler	1.1	5.3	28.4	46.4	25.0	50.6	79.8	14.5	13.2	30.7	67.5	21.3	23.0	46.7	79.6	15.7
Axis-Angle	4.2	13.7	42.1	35.0	21.4	53.6	82.1	14.0	15.8	32.5	73.7	19.6	25.7	42.8	81.6	16.6
Quaternion	9.5	23.2	54.7	27.1	45.2	64.9	86.9	10.5	18.4	32.5	78.9	18.9	25.7	51.3	81.6	14.3
S^2-Reg	18.9	42.1	66.3	16.7	70.2	85.7	98.2	7.7	28.9	56.1	86.8	13.6	38.8	56.6	78.9	13.3
5D	4.2	10.5	48.4	32.1	23.2	46.4	84.5	16.1	9.6	30.7	79.8	20.3	22.4	36.8	69.1	18.8
6D	12.6	18.9	52.6	29.0	44.0	67.3	89.3	11.4	11.4	36.8	88.6	17.2	30.9	50.7	85.5	14.7
SVD-Inf	17.9	31.6	56.8	23.3	56.5	76.2	91.1	8.9	21.9	47.4	86.8	15.6	30.3	52.6	86.2	14.3
SVD-Train	13.7	25.3	52.6	25.4	42.3	63.1	85.7	11.4	18.4	40.4	81.6	18.3	32.9	50.0	86.2	14.6